Radicals masquerading as electrophiles: a computational study of the intramolecular addition reactions of acyl radicals to imines†

Hiroshi Matsubara,[a] Chantal T. Falzon,[b] Ilhyong Ryu[a] and Carl H. Schiesser*[b,c]

Received 28th February 2006, Accepted 6th March 2006
First published as an Advance Article on the web 30th March 2006
DOI: 10.1039/b603024f

Ab initio calculations using 6-311G**, cc-pVDZ, and aug-cc-pVDZ, with (MP2, QCISD, CCSD(T)) and without (UHF) electron correlation, and density functional methods (BHandHLYP and B3LYP) predict that cyclization of the 5-aza-5-hexenoyl and (*E*)-6-aza-5-hexenoyl radicals proceed to afford the 5-*exo* products. At the CCSD(T)/cc-pVDZ//BHandHLYP/cc-pVDZ level of theory, energy barriers ($\Delta E^{\ddagger}$) of 36.1 and 47.0 kJ mol^{-1} were calculated for the 5-*exo* and 6-*endo* pathways for the cyclization of the 5-aza-5-hexenoyl radical. On the other hand, at the same level of theory, $\Delta E^{\ddagger}$ of 38.9 and 45.4 kJ mol^{-1} were obtained for the 5-*exo* and 6-*endo* cyclization modes of (*E*)-6-aza-5-hexenoyl radical, with exothermicities of about 27 and 110 kJ mol^{-1} calculated for the *exo* and *endo* modes, respectively. Under suitable experimental conditions, the 6-*endo* cyclization product is likely to dominate. Analysis of the molecular orbitals involved in these ring-closure reactions indicate that both reactions at nitrogen are assisted by dual orbital interactions involving simultaneous SOMO–π* and LP–π* overlap in the transitions states. Interestingly, the (*Z*)-6-aza-5-hexenoyl radical, that cannot benefit from these dual orbital effects is predicted to ring-close exclusively in the 5-*exo* fashion.

Introduction

Radical cyclization reactions have become part of repertoire of the synthetic organic chemist, even for the synthesis of nitrogen-containing heterocycles such as alkaloides.[1,2] The majority of examples that involve addition onto carbon–nitrogen double-bonds typically involve alkyl radicals and, to a lesser, extent vinyl radicals.[3] However, these systems are often plagued by poor selectivity.[4,5] For example, Bowman and his associates found that the phenylselenide **1** underwent addition at both ends of the imine π-system to yield five- and six-membered heterocycles in 42 and 18% yield, respectively (Scheme 1).[5]

Scheme 1

In 1998, Ryu and co-workers demonstrated that acyl radicals add readily to carbon–nitrogen multiple bonds with complete selectivity for the formation of the smaller heterocycle in which the acyl radicals attacked the nitrogen of the reacting imine.[6] For example, when the 3-bromopropylimine **2** was treated with carbon monoxide in the presence of tributyltin hydride and AIBN, 2-pyrrolidinone **3** was obtained in 81% yield (Scheme 2). Furthermore, additions onto a variety of imines invariably gave rise to the smaller heterocycle, with no trace of either the larger heterocycles in which acyl radical attack has occurred at the carbon end of the imine π-system, or directly reduced materials (Scheme 3).[6,7]

Scheme 2

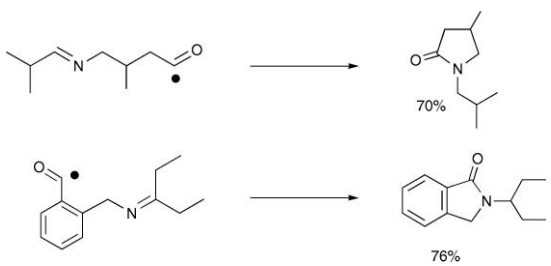

Scheme 3

The origin of this selectivity raises intriguing mechanistic questions. It is well known that acyl radicals are considered nucleophilic in the context of addition to C=C double bonds containing electron-withdrawing groups.[8] Within this in mind, the experimental observations seem contradictory because only products from attack of the acyl radical at the nucleophilic imine nitrogen are observed. In order to understand the intimate

[a]*Department of Chemistry, Graduate School of Science, Osaka Prefecture University, Sakai, Osaka, 599-8531, Japan*
[b]*School of Chemistry, The University of Melbourne, Victoria, Australia 3010*
[c]*Bio21 Molecular Science and Biotechnology Institute, The University of Melbourne, Victoria, Australia 3010. E-mail: carlhs@unimelb.edu.au; Fax: 61 3 9347 8189; Tel: 61 3 8344 2432*

† Electronic supplementary information (ESI) available: Gaussian archive entries for all structures in this study at all optimised levels of theory. BHandHLYP/6-311G** GaussView generated animations of the transition state vectors in **10** and (*E*)-**13** as audio video interleave (AVI) files. See DOI: 10.1039/b603024f

details surrounding this highly regioselective cyclization process, we sought recourse to *ab initio* and density functional techniques. We now report the results of computational investigations into the ring-closure reactions of 5-aza-5-hexenoyl (**4**) and 6-aza-5-hexenoyl radicals (**5**) (Scheme 4).[9]

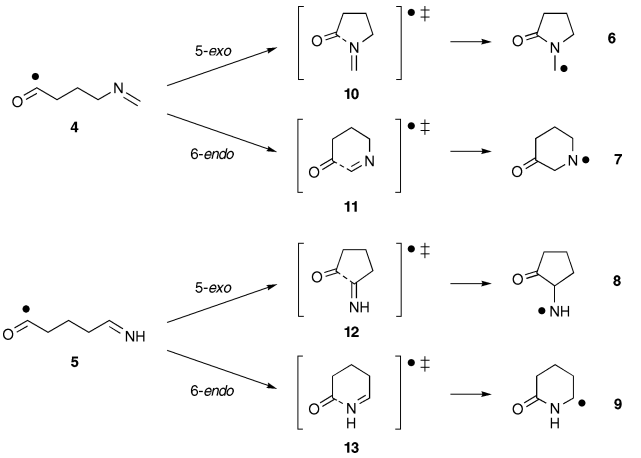

Scheme 4

Methods

Ab initio and DFT molecular orbital calculations were carried out on Compaq Personal Workstation 600au, Alpha Station DS10L, and Dell PowerEdge 400SC computers using the Gaussian 98 and Gaussian 03 program.[10,11] Geometry optimizations were performed using standard gradient techniques at the SCF, MP2, BHandHLYP and B3LYP levels of theory using restricted (RHF, RMP2, RBHandHLYP and RB3LYP) and unrestricted (UHF, UMP2, UBHandHLYP and UB3LYP) methods for closed- and open-shell systems, respectively.[12] In every case, standard basis sets were used. All ground and transition states were verified by vibrational frequency analysis. Further single-point QCISD and CCSD(T) calculations were performed on each of the MP2, BHandHLYP and B3LYP optimized structures. When correlated methods were used, calculations were carried out using the frozen core approximation. Values of $\langle s^2 \rangle$ never exceeded 0.86 before annihilation of quartet contamination (except for some UHF calculations) and were mostly 0.79 at correlated levels of theory. Where appropriate, zero-point vibrational energy (ZPE) corrections have been applied. Natural bond orbital (NBO) analyses[13] were performed within the Gaussian 03 program.

Optimized geometries and energies for all transition structures in this study (Gaussian archive entries) are available in the ESI.

Results and discussion

Intramolecular addition reactions of the 5-aza-5-hexenoyl radical (4)

Extensive searching of the C_5H_8NO potential energy surface at the UHF/6-311G**, MP2/6-311G**, MP2/cc-pVDZ, BHandHLYP/6-311G**, BHandHLYP/cc-pVDZ, B3LYP/6-311G**, and B3LYP/cc-pVDZ levels of theory located transition states **10** and **11** for the 5-*exo* and 6-*endo* ring-closure reactions involving the 5-aza-5-hexenoyl radical (**4**) (Scheme 4). Analysis of the appropriate force constants provided computational evidence for these structures as being true transition states. The important geometric features of transition states **10** and **11** are summarized in Fig. 1, while calculated energy barriers ($\Delta E_1^{\ddagger}$ and $\Delta E_2^{\ddagger}$, Scheme 5) together with the corresponding imaginary frequencies are listed in Table 1. Full computational details are available in the ESI.

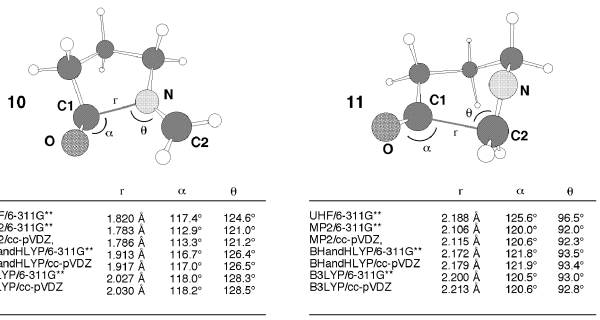

	r	α	θ
UHF/6-311G**	1.820 Å	117.4°	124.6°
MP2/6-311G**	1.783 Å	112.9°	121.0°
MP2/cc-pVDZ,	1.786 Å	113.3°	121.2°
BHandHLYP/6-311G**	1.913 Å	116.7°	126.4°
BHandHLYP/cc-pVDZ	1.917 Å	117.0°	126.5°
B3LYP/6-311G**	2.027 Å	118.0°	128.3°
B3LYP/cc-pVDZ	2.030 Å	118.2°	128.5°

	r	α	θ
UHF/6-311G**	2.188 Å	125.6°	96.5°
MP2/6-311G**	2.106 Å	120.0°	92.0°
MP2/cc-pVDZ,	2.115 Å	120.6°	92.3°
BHandHLYP/6-311G**	2.172 Å	121.8°	93.5°
BHandHLYP/cc-pVDZ	2.179 Å	121.9°	93.4°
B3LYP/6-311G**	2.200 Å	120.5°	93.0°
B3LYP/cc-pVDZ	2.213 Å	120.6°	92.8°

Fig. 1 Optimized structures of transition states **10** and **11** for the 5-*exo* and 6-*endo* cyclization reactions of 5-aza-5-hexenoyl radical (**4**).

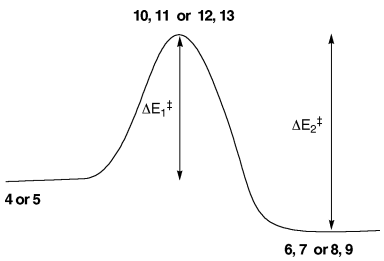

Scheme 5

Inspection of the transition structures shown in Fig. 1, reveals that the *endo* structure **11** adopts a boat-like conformation, that resembles other radical 6-*endo* cyclizations.[14] Surprisingly, the *exo* structure **10** adopts a chair-like conformation, in which the imine π-system is not orientated in a manner that allows the radical SOMO to overlap efficiently, rather it appears that the nitrogen lone-pair is predominantly directed toward the acyl carbonyl. Indeed, dihedral angles between the carbonyl and imine groups are predicted to be very different, with values lying in the range: 24.0 to 51.8° (**10**) and 109.0 to 138.3° (**11**), respectively. Further examination of these structures indicate that the transition state separations located for the *endo* pathway are significantly larger than those located for the *exo* pathway, at all levels employed. This is perhaps not unexpected as it is a reflection of the differences between carbon–carbon and carbon–nitrogen σ-bond lengths. The transition state separations are predicted to be 1.783–2.030 Å for the *exo* pathways, compared to 2.106–2.213 Å for the *endo* pathways. In addition, the angles (α) located around the carbonyl π-system (O–C1–X) are calculated to be much wider in **11** (X = C2) than those in **10** (X = N). At the MP2/cc-pVDZ level of theory the angles (α) located for structure **10** and **11** are predicted to be 113.3 and 120.6°, respectively, while angles of 117.0° (**10**) and 121.9° (**11**) were located at the BHandHLYP/cc-pVDZ level of theory. B3LYP/cc-pVDZ calculations predict these angles to be 118.2° (**10**) and 120.6° (**11**) for the *exo* and *endo* pathways, respectively.

Table 1 Calculated energy barriers[a] for the forward ($\Delta E_1^{\ddagger}$) and reverse ($\Delta E_2^{\ddagger}$) cyclization reactions of 5-aza-5-hexenoyl radical (**4**) and imaginary frequencies (ν)[b] of transition states **10** and **11**

	10					**11**				
Method	$\Delta E_1^{\ddagger}$	$\Delta E_1^{\ddagger}$ +ZPE	$\Delta E_2^{\ddagger}$	$\Delta E_2^{\ddagger}$ +ZPE	ν	$\Delta E_1^{\ddagger}$	$\Delta E_1^{\ddagger}$ +ZPE	$\Delta E_2^{\ddagger}$	$\Delta E_2^{\ddagger}$ +ZPE	ν
UHF/6-311G**	74.5	71.3	199.7	191.7	653i	64.5	61.4	141.4	131.0	437i
MP2/6-311G**	62.7	51.8	184.0	184.5	512i	86.0	70.3	127.2	122.2	715i
MP2/cc-pVDZ	64.4	51.7	185.7	185.9	567i	86.8	69.3	129.4	123.7	701i
MP2/aug-cc-pVDZ//MP2/cc-pVDZ	49.5	—	175.5	—	—	78.0	—	126.3	—	—
QCISD/cc-pVDZ//MP2/cc-pVDZ	57.3	—	167.4	—	—	60.7	—	113.5	—	—
CCSD(T)/cc-pVDZ//MP2/cc-pVDZ	54.2	—	162.9	—	—	57.0	—	106.2	—	—
BHandHLYP/6-311G**	40.0	39.7	177.5	172.4	509i	52.9	52.0	121.1	113.5	474i
BHandHLYP/cc-pVDZ	39.8	39.2	178.7	173.6	517i	52.2	51.0	125.4	117.6	465i
BHandLYP/aug-cc-pVDZ//BHandHLYP/cc-pVDZ	36.8	—	177.1	—	—	47.6	—	124.9	—	—
QCISD/cc-pVDZ//BHandHLYP/cc-pVDZ	36.3	—	176.6	—	—	53.0	—	124.4	—	—
CCSD(T)/cc-pVDZ//BHandHLYP/cc-pVDZ	36.1	—	176.6	—	—	47.0	—	124.0	—	—
B3LYP/6-311G**	22.3	22.1	149.2	143.4	356i	42.4	42.1	99.5	85.7	372i
B3LYP/cc-pVDZ	21.2	20.9	150.8	145.0	353i	41.3	40.8	97.2	90.5	358i
B3LYP/aug-cc-pVDZ//B3LYP/cc-pVDZ	20.5	—	150.0	—	—	37.0	—	92.3	—	—
QCISD/cc-pVDZ//B3LYP/cc-pVDZ	20.1	—	149.5	—	—	36.9	—	92.1	—	—
CCSD(T)/cc-pVDZ//B3LYP/cc-pVDZ	19.9	—	149.5	—	—	36.5	—	91.7	—	—

[a] Energies in kJ mol^{-1}. [b] Frequencies in cm^{-1}.

As shown in Table 1, for both the *exo* and *endo* pathways, calculated energy barriers ($\Delta E_2^{\ddagger}$) for the reverse (ring-opening) reactions (Scheme 5) are always larger than those ($\Delta E_1^{\ddagger}$) for the forward (cyclization) process; these reactions are predicted to be exothermic at all levels of theory employed in this study. For example, the energy barrier ($\Delta E_1^{\ddagger}$) for the *exo* and *endo* cyclization pathways are calculated to be 74.5 and 64.5 kJ mol^{-1}, respectively, at the UHF/6-311G** level of theory, indicating that the *endo* pathway is energetically favoured by 10 kJ mol^{-1}. As expected, electron correlation is important in these calculations; MP2/6-311G** serves to alter these energy barriers to 62.7 and 86.0 kJ mol^{-1} for the *exo* and *endo* cyclizations, respectively. Interestingly, calculations with electron correlation employed here afford lower energy barriers ($\Delta E_1^{\ddagger}$) for the *exo* pathways than those for the *endo* pathways, which is good agreement with the experimental observations.[6] Inclusion of zero-point vibrational energy correction (ZPE) serves to decrease these barriers by about 10 kJ mol^{-1}. At the CCSD(T)/cc-pVDZ//MP2/cc-pVDZ level of theory, the energy barriers ($\Delta E_1^{\ddagger}$) located for the *exo* and *endo* pathways are predicted to be at 54.2 and 57.0 kJ mol^{-1}, respectively, with the *exo* pathway energetically favoured by only 2.8 kJ mol^{-1}. In contrast, when DFT methods were employed for geometry optimizations, the predominance of the *exo* pathway is further increased. For example, at the CCSD(T)/cc-pVDZ//BHandHLYP/cc-pVDZ level of theory, the energy barriers located for the *exo* and the *endo* pathways are predicted to be 36.1 and 47.0 kJ mol^{-1}, respectively, with the *exo* pathway preferred by 10.9 kJ mol^{-1}, while the CCSD(T)/cc-pVDZ//B3LYP/cc-pVDZ calculations predicted 19.9 and 36.5 kJ mol^{-1} of energy barriers for these same two reactions, respectively, with the *exo* pathway energetically favoured by 16.6 kJ mol^{-1}. It is interesting to note that the B3LYP and higher single-point calculations of the structures optimized by the B3LYP level of theory afford significantly lower energy barriers. These observations suggest that significant enough differences between the MP2 and B3LYP surfaces might exist as to affect the single-point calculations reported above. As we have note previously, we urge the use of caution in the use of B3LYP for the study of radical reactions.[9,15]

Mechanistic insight into the cyclization of the 5-aza-5-hexenoyl radical

As already witnessed, the 5-*exo* and 6-*endo* cyclizations require addition of the acyl radical at the appropriate end of the imine π-system to afford the new σ-bond. In order to provide further insight into the mechanism of the cyclization, we examined more closely the environment about the forming bonds within each the transition state.

When the cyclization proceeds in the *exo* mode, addition is required to take place onto the nitrogen atom. This raises some interesting mechanistic issues, as both the SOMO and the nitrogen lone-pair are able to participate in the bond-formation process. Consequently, as shown in Scheme 6, there are two main methods of cyclization available: 5-*exo* homolytic addition onto the imine nitrogen atom (Path A—the "standard" free-radical process) or nucleophilic addition by the imine nitrogen atom onto the carbonyl carbon of the acyl radical (Path B).

Inspection of the motion vectors associated with the transition state (**10**) reveals some interesting features (Fig. 2). When

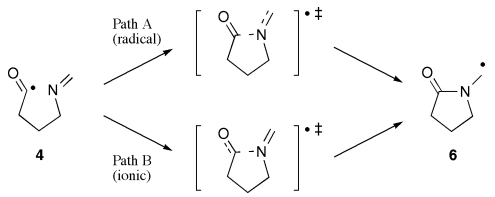

Scheme 6

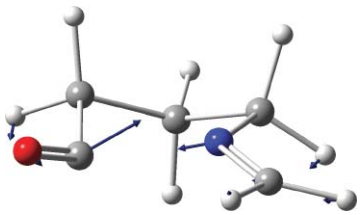

Fig. 2 BH and HLYP/6-311G** generated motion vectors for transition state **10**.

animated, the acyl carbon in **10** appears to swing above the imine nitrogen during bond formation, as indicated by the motion arrows in the structure of **10**.† These unusual observations prompted us to look more closely at the molecular orbitals involved in this intramolecular homolytic addition process.

Visualisation of the Kohn–Sham orbitals generated at the BHandHLYP/6-311G** level of theory reveals the origin of the unexpected motion in transition state **10**. Not unexpectedly, the transition state "SOMO" comprises interaction of the unpaired electron in the acyl radical with the imine π* orbital. Somewhat surprisingly however, of similar energy is a second orbital interaction comprising interaction of the nitrogen lone pair with the acyl radical π* orbital (Fig. 3).

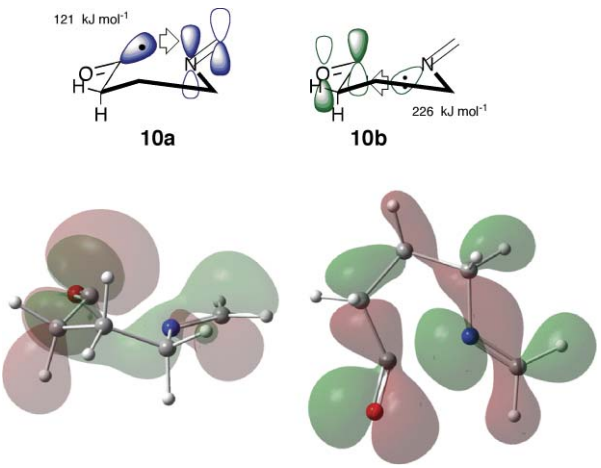

Fig. 3 Kohn–Sham SOMO–π (left) and LP–π* (right) interactions in transition state **10**.

Natural bond orbital (NBO) analysis at the BHandHLYP/6-311G** level of theory reveals that the SOMO–π* overlap depicted in **10a** is worth about 120 kJ mol^{-1}, with the LP–π* interaction (**10b**) worth some 225 kJ mol^{-1}. These calculations indicate clearly that both radical and nucleophilic interactions operate during that 5-*exo* ring-closure of **4** and that the nucleophilic character of the imine dominates over the radical interaction in the transition state. We have reported recently similar observations for intermolecular homolytic addition of radicals that can also act as electrophiles with both imine and carbonyl π-systems.[16]

Intramolecular addition reactions of the 6-aza-5-hexenoyl radical

Extensive searching of the C_5H_8NO potential energy surfaces at the same levels of theory employed above located transition states **12** and **13** for the *exo* and *endo* pathways of the intramolecular addition reactions of the (*E*)- and (*Z*)-isomers of the 6-aza-5-hexenoyl radical (Scheme 4). Analysis of the appropriate force constants provided computational evidence for these structures as being true transition states. The important geometric features of transition states **12** and **13** are summarized in Fig. 4, while calculated energy barriers ($\Delta E_1^{\ddagger}$ and $\Delta E_2^{\ddagger}$, Scheme 5) together with the corresponding imaginary frequencies are listed in Tables 2 and 3. Full computational details are available in the ESI.

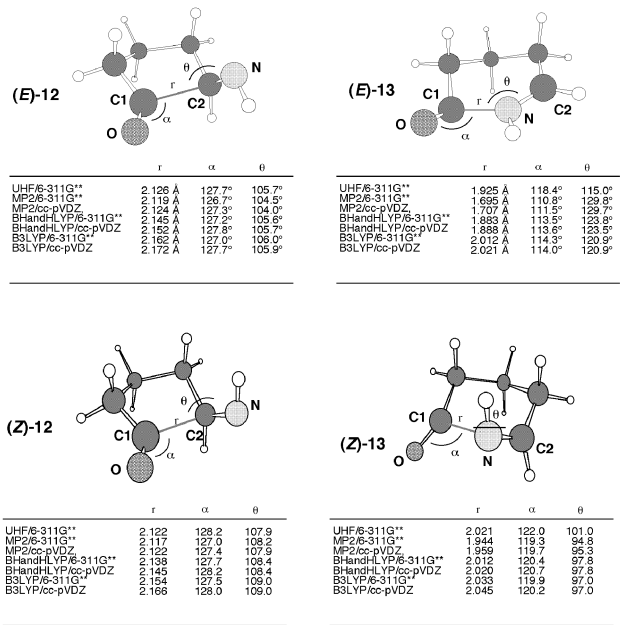

Fig. 4 Optimized structures of transition states **12** and **13** for the 5-*exo* and 6-*endo* cyclization reactions of the (*E*)- and (*Z*)-isomers of the 6-aza-5-hexenoyl radical (**5**).

Inspection of Fig. 4 reveals that the *exo* structure (*E*)-**12** adopts a chair-like conformation, which resembles typical radical 5-*exo* cyclizations. The *endo* structure (*E*)-**13** also adopts a chair-like conformation; however, the geometry about the forming bond bears a striking resemblance to that in transition state **10**; that is, the imine π-system in this structure is not orientated in a manner that allows the radical SOMO to overlap efficiently, rather it appears that the nitrogen lone-pair is predominantly directed toward the acyl carbonyl carbon. Similarly, the structure around the forming bond in the *exo* structure (*E*)-**12** is calculated to be close to that in transition state **11** despite any conformational differences. In short, the geometrical trends observed in **10** and **11** can be seen in (*E*)-**13** and (*E*)-**12**, respectively. For example, the transition state separations located for the *exo* pathway ((*E*)-**12**: 2.119–2.172 Å) are significantly wider than those located for the *endo* pathway ((*E*)-**13**: 1.695–2.021 Å). In addition, the angles located around the carbonyl π-system (O–C1–X) are calculated

Table 2 Calculated energy barriers[a] for the forward ($\Delta E_1^{\ddagger}$) and reverse ($\Delta E_2^{\ddagger}$) cyclization reactions of (*E*)-6-aza-5-hexenoyl radical ((*E*)-**5**) and imaginary frequencies (ν)[b] of transition states (*E*)-**12** and (*E*)-**13**

	(*E*)-**12**					(*E*)-**13**				
Method	$\Delta E_1^{\ddagger}$	$\Delta E_1^{\ddagger}$ +ZPE	$\Delta E_2^{\ddagger}$	$\Delta E_2^{\ddagger}$ +ZPE	ν	$\Delta E_1^{\ddagger}$	$\Delta E_1^{\ddagger}$ +ZPE	$\Delta E_2^{\ddagger}$	$\Delta E_2^{\ddagger}$ +ZPE	ν
UHF/6-311G**	53.7	51.0	105.4	98.9	459i	80.0	77.6	202.0	190.3	833i
MP2/6-311G**	70.4	64.5	93.4	91.0	586i	64.5	65.1	182.4	180.1	622i
MP2/cc-pVDZ	70.9	57.3	95.1	92.9	587i	64.6	57.2	185.0	182.0	701i
MP2/aug-cc-pVDZ//MP2/cc-pVDZ	66.5	—	89.7	—	—	52.5	—	172.2	—	—
QCISD/cc-pVDZ//MP2/cc-pVDZ	46.6	—	75.6	—	—	56.7	—	168.9	—	—
CCSD(T)/cc-pVDZ//MP2/cc-pVDZ	43.1	—	69.9	—	—	53.1	—	164.5	—	—
BHandHLYP/6-311G**	39.8	38.9	80.8	76.5	400i	43.8	45.3	182.0	174.2	590i
BHandHLYP/cc-pVDZ	37.8	36.9	84.7	80.3	397i	40.2	41.8	184.5	176.5	582i
BHandLYP/aug-cc-pVDZ//BHandHLYP/cc-pVDZ	38.6	—	82.3	—	—	44.3	—	181.7	—	—
QCISD/cc-pVDZ//BHandHLYP/cc-pVDZ//BHandHLYP/cc-pVDZ	43.1	—	73.7	—	—	51.1	—	165.0	—	—
CCSD(T)/cc-pVDZ//BHandHLYP/cc-pVDZ//BHandHLYP/cc-pVDZ	38.9	—	67.7	—	—	45.4	—	158.8	—	—

[a] Energies in kJ mol^{-1}. [b] Frequencies in cm^{-1}.

Table 3 Calculated energy barriers[a] for the forward ($\Delta E_1^{\ddagger}$) and reverse ($\Delta E_2^{\ddagger}$) cyclization reactions of (*Z*)-6-aza-5-hexenoyl radical ((*Z*)-**5**) and imaginary frequencies (ν)[b] of transition states (*Z*)-**12** and (*Z*)-**13**

	(*Z*)-**12**					(*Z*)-**13**				
Method	$\Delta E_1^{\ddagger}$	$\Delta E_1^{\ddagger}$ +ZPE	$\Delta E_2^{\ddagger}$	$\Delta E_2^{\ddagger}$ +ZPE	ν	$\Delta E_1^{\ddagger}$	$\Delta E_1^{\ddagger}$ +ZPE	$\Delta E_2^{\ddagger}$	$\Delta E_2^{\ddagger}$ +ZPE	ν
UHF/6-311G**	59.9	55.9	99.3	93.5	464i	105.6	104.5	233.0	222.4	580i
MP2/6-311G**	75.5	69.5	86.6	85.2	577i	114.0	110.4	237.1	230.4	1098i
MP2/cc-pVDZ	75.8	71.8	86.2	84.9	577i	112.9	111.4	236.5	229.6	1049i
MP2/aug-cc-pVDZ//MP2/cc-pVDZ	71.8	—	84.0	—	—	108.7	—	233.0	—	—
QCISD/cc-pVDZ//MP2/cc-pVDZ	50.3	—	65.8	—	—	89.7	—	205.2	—	—
CCSD(T)/cc-pVDZ//MP2/cc-pVDZ	47.1	—	59.9	—	—	81.7	—	195.9	—	—
BHandHLYP/6-311G**	44.8	43.7	72.0	68.6	296i	85.0	86.3	227.9	219.9	664i
BHandHLYP/cc-pVDZ	42.2	41.2	74.0	70.6	391i	80.6	82.1	228.4	220.2	644i
QCISD/cc-pVDZ//BHandHLYP/cc-pVDZ//BHandHLYP/cc-pVDZ	47.1	—	64.1	—	—	83.0	—	200.1	—	—
CCSD(T)/cc-pVDZ//BHandHLYP/cc-pVDZ//BHandHLYP/cc-pVDZ	42.9	—	57.7	—	—	74.9	—	191.5	—	—

[a] Energies in kJ mol^{-1}. [b] Frequencies in cm^{-1}.

to be much wider in **10** (X = C2) than those in **11** (X = N). At the MP2/cc-pVDZ level of theory the O–C1–X angles located for structure **10** and **11** are predicted to be 127.3 and 111.5°, respectively, while angles of 127.8°((*E*)-**12**) and 113.6° ((*E*)-**13**), and 127.7° ((*E*)-**12**) and 114.0° ((*E*)-**13**) were located at the BHandHLYP/cc-pVDZ and B3LYP/cc-pVDZ levels of theory, respectively.

Once again, inspection of the transition state motion vectors† and the Kohn–Sham orbitals calculated at the BHandHLYP/6-311G** reveals the same interesting dual orbital effect operating in transition state ((*E*)-**13**) as was observed in (**10**) (Fig. 5).

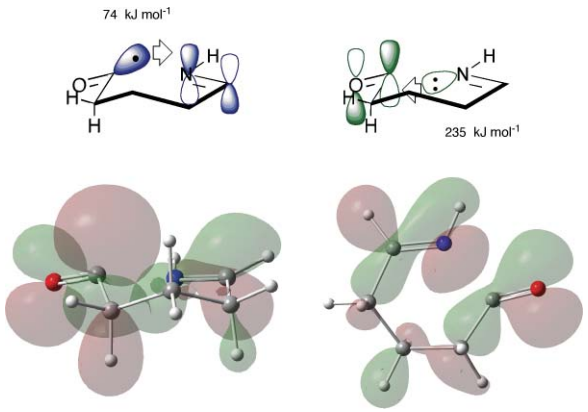

Fig. 5 Kohn–Sham SOMO–π* (left) and LP–π* (right) interactions in transition state (*E*)-**13**.

Table 2 shows that in both *exo* and *endo* pathways, these reactions are calculated to be exothermic at all levels of theory employed in this study. Once again, calculations that include electron correlation generally afford lower energy barriers. For example, at the CCSD(T)/cc-pVDZ//MP2/cc-pVDZ level of theory, the energy barriers located for the *exo* and the *endo* pathways are predicted to be 43.1 and 53.1 kJ mol^{-1}, respectively, with the *exo* pathway preferred by 10.0 kJ mol^{-1}, while the CCSD(T)/cc-pVDZ//BHandHLYP/cc-pVDZ calculations provide values of 38.9 and 45.4 kJ mol^{-1}, respectively, with the *exo* pathway favoured by only 6.5 kJ mol^{-1}.

What is clear from the calculated data is that, while the *exo* reaction is significantly less exothermic than the corresponding *endo* process, the former reaction is still favoured slightly from a kinetic perspective. However, with a calculated exothermicities around 27 kJ mol^{-1} at some levels of theory, it is likely that the *endo* product will be formed through reversible *exo* addition competing with irreversible *endo* addition, although the exact outcome of this competition would depend on the concentration of any radical trap (*e.g.* Bu_3SnH) used. These predicted outcomes to be compared with recent experimental data from our laboratories, in which the cyclization of the (*E*)-6-aza-7-ethyl-5-octenoyl radical (**14**) was demonstrated to afford 1-(3-pentyl)-2-piperdinone exclusively (Scheme 7),[17] however, it should be noted that the alkyl substituent

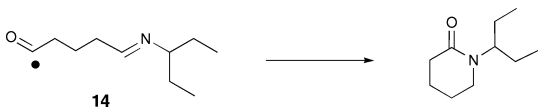

Scheme 7

on nitrogen is likely to favour *endo* attack from an electronic perspective, pushing **14** further in the *endo* direction when compared with (*E*)-**5**. We are currently further investigating the effect of substitution on these interesting reactions.

It is of interest to compare the calculations to this point with those for the cyclization of the stereoisomeric (*Z*)-6-aza-5-hexenoyl radical. The data presented in Fig. 4 and Table 3 clearly indicate that unlike its (*E*)-isomer, the (*Z*)-6-aza-5-hexenoyl system ((*Z*)-**5**) is predicted to cyclize exclusively in the *exo* mode, with energy barriers ($\Delta E_1^{\ddagger}$) for the *exo* mode lying between about 42 and 76 kJ mol^{-1} depending on the level of theory, some 40 kJ mol^{-1} lower that the corresponding barrier for the *endo* mode of attack (Table 3).

Inspection of Fig. 4 and 6 provides a clear explanation for the differences observed for these two geometrical isomers. While the *exo* mode of cyclization *via* transition state **12** is largely unaffected by the geometry about the imine π-system, the same cannot be said for the *endo* mode of attack. While (*E*)-**13** can benefit by the dual orbital effect described above, the geometry about the imine π-bond in the (*Z*)-system renders it impossible for the analogous LP–π* interaction to become effective in the ring-closure transitions state (*Z*)-**13** (Fig. 6). As a consequence, the cyclization of the (*Z*)-6-aza-5-hexenoyl radical is purely governed by the SOMO–π* interaction. The lack of the (additional) LP–π* during cyclization, out of necessity, leads to higher energy barriers for ring-closure. Given that both (*E*)- and (*Z*)-isomers of the 6-aza-5-hexenoyl radical (**5**) are calculated to have similar energy barriers for *exo* cyclization (*viz.* 40 and 45 kJ mol^{-1}, respectively) to afford the substituted cyclopentane, these calculations suggest that the LP–π* available in (*E*)-**13**, and lost to (*Z*)-**13**, is worth some 40 kJ mol^{-1}.

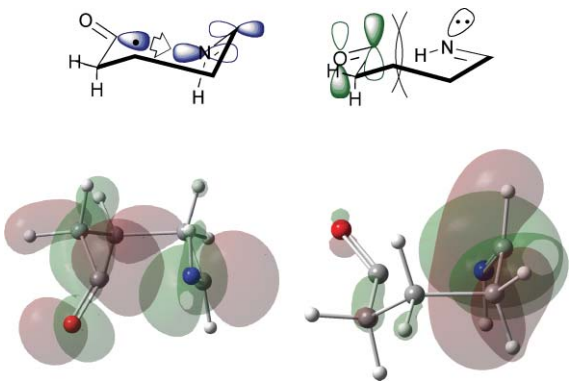

Fig. 6 Kohn–Sham SOMO–π* interactions (left) and nitrogen LP (right) in transition state (*Z*)-**13**.

Conclusions

We have demonstrated that intramolecular homolytic addition reactions of acyl radicals onto imines can proceed in both *exo* and *endo* modes, depending on the ring-size involved and geometry of the imine moiety. Unless steric interactions prevail, addition to the nitrogen end of the imine π-system involves dual orbital interactions involving both SOMO–π* and LP–π* interactions in which the latter interaction can dominate. We conclude that acyl radicals derive significant energy benefit by masquerading as electrophiles in reactions with imines.

Acknowledgements

We gratefully acknowledge the support of the Melbourne Advanced Research Computing Centre and the Victorian Institute for Chemical Sciences High Performance Computing Facility. Support from the Australian Research Council through the Centres of Excellence Program is gratefully acknowledged.

References

1 For leading reviews, see: *Radicals in Organic Synthesis, vol. 1–2*, ed. P. Renaud and M. P. Sibi, Wiley-VCH, Weiheim, 2001.
2 For some recent reports, see: W. R. Bowman, M. O. Cloonan and S. L. Krintel, *J. Chem. Soc., Perkin Trans. 1*, 2001, 2885.
3 G. K. Friestad, *Tetrahedron*, 2001, **57**, 5461; A. G. Fallis and I. M. Brinza, *Tetrahedron*, 1997, **53**, 17543.
4 W. R. Bowman, P. T. Stephenson, N. K. Terett and A. R. Young, *Tetrahedron*, 1995, **51**, 7959; M. J. Tomazewski and J. Warkentin, *Tetrahedron Lett.*, 1992, **33**, 2123; L. S. Lee, S. Kim and S. Lee, *J. Am. Chem. Soc.*, 1991, **113**, 9882; A. Kijima, K. Ogasawara, S. Takano and M. Suzuki, *Heterocycles*, 1994, **37**, 149.
5 W. R. Bowman, P. T. Stephenson, N. K. Terett and A. R. Young, *Tetrahedron Lett.*, 1994, **35**, 6369.
6 I. Ryu, K. Matsu, S. Minakata and M. Komatsu, *J. Am. Chem. Soc.*, 1998, **120**, 5838.
7 I. Ryu, H. Miyazato, H. Kuriyama, K. Matsu, M. Tojino, T. Fukuyama, S. Minakata and M. Komatsu, *J. Am. Chem. Soc.*, 2003, **125**, 5632; M. Tojino, N. Ostuka, T. Fukuyama, H. Matsubara, C. H. Schiesser, H. Kuriyama, H. Miyazato, S. Minakata, M. Komatsu and I. Ryu, *Org. Biomol. Chem.*, 2003, **1**, 4262.
8 C. Chatgilialoglu, D. Crich, M. Komatsu and I. Ryu, *Chem. Rev.*, 1999, **99**, 1991.
9 This work has been published in preliminary form, see: C. T. Falzon, I. Ryu and C. H. Schiesser, *Chem. Commun.*, 2002, 2338.
10 M. J. Frisch, G. W. Trucks, H. B. Schlegel, G. E. Scuseria, M. A. Robb, J. R. Cheeseman, V. G. Zakrzewski, J. A. Montgomery, Jr., R. E. Stratmann, J. C. Burant, S. Dapprich, J. M. Millam, A. D. Daniels, K. N. Kudin, M. C. Strain, O. Farkas, J. Tomasi, V. Barone, M. Cossi, R. Cammi, B. Mennucci, C. Pomelli, C. Adamo, S. Clifford, J. Ochterski, G. A. Petersson, P. Y. Ayala, Q. Cui, K. Morokuma, D. K. Malick, A. D. Rabuck, K. Raghavachari, J. B. Foresman, J. Cioslowski, J. V. Ortiz, A. G. Baboul, B. B. Stefanov, G. Liu, A. Liashenko, P. Piskorz, I. Komaromi, R. Gomperts, R. L. Martin, D. J. Fox, T. Keith, M. A. Al-Laham, C. Y. Peng, A. Nanayakkara, C. Gonzalez, M. Challacombe, P. M. W. Gill, B. G. Johnson, W. Chen, M. W. Wong, J. L. Andres, M. Head-Gordon, E. S. Replogle and J. A. Pople, *GAUSSIAN 98 (Revision A.7)*, Gaussian, Inc., Pittsburgh, PA, 1998.
11 M. J. Frisch, G. W. Trucks, H. B. Schlegel, G. E. Scuseria, M. A. Robb, J. R. Cheeseman , J. A. Montgomery, Jr., T. Vreven, K. N. Kudin, J. C. Burant, J. M. Millam, S. S. Iyengar, J. Tomasi, V. Barone, B. Mennucci, M. Cossi, G. Scalmani, N. Rega, G. A. Petersson, H. Nakatsuji, M. Hada, M. Ehara, K. Toyota, R. Fukuda, J. Hasegawa, M. Ishida, T. Nakajima, Y. Honda, O. Kitao, H. Nakai, M. Klene, X. Li, J. E. Knox, H. P. Hratchian, J. B. Cross, C. Adamo, J. Jaramillo, R. Gomperts, R. E. Stratmann, O. Yazyev, A. J. Austin, R. Cammi, C. Pomelli, J. W. Ochterski, P. Y. Ayala, K. Morokuma, G. A. Voth, P. Salvador, J. J. Dannenberg, V. G. Zakrzewski, S. Dapprich, A. D. Daniels, M. C. Strain, O. Farkas, D. K. Malick, A. D. Rabuck, K. Raghavachari, J. B. Foresman, J. V. Ortiz, Q. Cui, A. G. Baboul, S. Clifford, J. Cioslowski, B. B. Stefanov, G. Liu, A. Liashenko, P. Piskorz, I. Komaromi, R. L. Martin, D. J. Fox, T. Keith, M. A. Al-Laham, C. Y. Peng, A. Nanayakkara, M. Challacombe, P. M. W. Gill, B. Johnson, W. Chen, M. W. Wong, C. Gonzalez and J. A. Pople, *GAUSSIAN 03 (Revision B.04)*, Gaussian, Inc., Pittsburgh, PA, 2003.
12 W. J. Hehre, L. Radom, P. v. R. Schleyer and P. A. Pople, Ab Initio *Molecular Orbital Theory*, Wiley, New York, 1986.
13 *NBO version 3.1*, E. D. Glendening, A. E. Reed, J. E. Carpenter and F. Weinhold.
14 A. G. Leach, R. Wang, G. E. Wohlhieter, S. I. Khan, M. E. Jung and K. N. Houk, *J. Am. Chem. Soc.*, 2003, **125**, 4271; C. Chatgilialoglu, C. Ferreri, M. Lucarini, A. Venturini and A. A. Zavitsas, *Chem.–Eur. J.*, 1997, **3**, 376.
15 T. Morihovitis, C. H. Schiesser and M. A. Skidmore, *J. Chem. Soc., Perkin Trans. 2*, 1999, 2041.
16 C. H. Schiesser, H. Matsubara, I. Ritsner and U. Wille, *Chem. Commun.*, 2006, 1067.
17 M. Tojino, N. Otsuka, T. Fukuyama, H. Matsubara and I. Ryu, unpublished.

